Published in final edited form as:
Neuroimage. 2014 October ; 99: 69–79. doi:10.1016/j.neuroimage.2014.05.033.

Evaluation of the Agonist PET Radioligand [^{11}C]GR103545 to Image Kappa Opioid Receptor in Humans: Kinetic Model Selection, Test-Retest Reproducibility and Receptor Occupancy by the Antagonist PF-04455242

Mika Naganawa[1,*], **Leslie K. Jacobsen**[2], **Ming-Qiang Zheng**[1], **Shu-Fei Lin**[1], **Anindita Banerjee**[2], **Wonkyung Byon**[2], **David Weinzimmer**[1], **Giampaolo Tomasi**[1], **Nabeel Nabulsi**[1], **Sarah Grimwood**[2], **Lori L. Badura**[2], **Richard E. Carson**[1], **Timothy J. McCarthy**[2], and **Yiyun Huang**[1]

[1]PET Center, Department of Diagnostic Radiology, Yale University School of Medicine, New Haven, CT, USA

[2]Pfizer Inc., Groton, CT and Cambridge, MA, USA

Abstract

Introduction—Kappa opioid receptors (KOR) are implicated in several brain disorders. In this report, a first-in-human Positron Emission Tomography (PET) study was conducted with the potent and selective KOR agonist tracer, [^{11}C]GR103545, to determine an appropriate kinetic model for analysis of PET imaging data and assess the test-retest reproducibility of model-derived binding parameters. The non-displaceable distribution volume (V_{ND}) was estimated from a blocking study with naltrexone. In addition, KOR occupancy of PF-04455242, a selective KOR antagonist that is active in preclinical models of depression, was also investigated.

Methods—For determination of a kinetic model and evaluation of test-retest reproducibility, 11 subjects were scanned twice with [^{11}C]GR103545. Seven subjects were scanned before and 75 min after oral administration of naltrexone (150 mg). For the KOR occupancy study, six subjects were scanned at baseline and 1.5 h and 8 h after an oral dose of PF-04455242 (15 mg, n = 1 and 30 mg, n = 5). Metabolite-corrected arterial input functions were measured and all scans were 150 min in duration. Regional time-activity curves (TACs) were analyzed with 1- and 2-tissue compartment models (1TC and 2TC) and the multilinear analysis (MA1) method to derive regional volume of distribution (V_T). Relative test-retest variability (TRV), absolute test-retest variability (aTRV) and intra-class coefficient (ICC) were calculated to assess test-retest reproducibility of regional V_T. Occupancy plots were computed for blocking studies to estimate occupancy and V_{ND}. The half maximal inhibitory concentration (IC_{50}) of PF-04455242 was

[*]Corresponding author: Mika Naganawa, +1-203-737-5582, mika.naganawa@yale.edu, Yale University, PET Center, 801 Howard Avenue, PO Box 208048, New Haven, CT, USA, 06520-8048.

determined from occupancies and drug concentrations in plasma. [^{11}C]GR103545 *in vivo* K_D was also estimated.

Results—Regional TACs were well described by the 2TC model and MA1. However, 2TC V_T was sometimes estimated with high standard error. Thus MA1 was the model of choice. Test-retest variability was ~15%, depending on the outcome measure. The blocking studies with naltrexone and PF-04455242 showed that V_T was reduced in all regions; thus no suitable reference region is available for the radiotracer. V_{ND} was estimated reliably from the occupancy plot of naltrexone blocking (V_{ND} = 3.4 ± 0.9 mL/cm^3). The IC_{50} of PF-04455242 was calculated as 55 ng/mL. [^{11}C]GR103545 *in vivo* K_D value was estimated as 0.069 nmol/L.

Conclusions—[^{11}C]GR103545 PET can be used to image and quantify KOR in humans, although it has slow kinetics and variability of model-derived kinetic parameters is higher than desirable. This tracer should be suitable for use in receptor occupancy studies, particularly those that target high occupancy.

Keywords

^{11}C-GR103545; PF-04455242; Kappa opioid receptor; Positron emission tomography (PET); Test-retest; occupancy plot

INTRODUCTION

Opioid receptors belong to the superfamily of G-protein coupled receptors and are classified into at least four subtypes: μ (MOR), δ (DOR), κ (KOR), and nociceptin (Corbett et al., 2006). KOR exist abundantly in the human brain, and have been implicated in a number of disorders, including substance abuse (Mash and Staley, 1999; Mello and Negus, 2000), epilepsy (de Lanerolle et al., 1997; Loacker et al., 2007), Alzheimer's disease (Mathieu-Kia et al., 2001), and major depression (Barber and Gottschlich, 1997; Gerra et al., 2006; Tenore, 2008). For example, multiple lines of evidence point to the involvement of KOR in depression and related mood disorders (Beardsley et al., 2005; Carlezon et al., 2006; Mague et al., 2003; McLaughlin et al., 2003; Newton et al., 2002; Reindl et al., 2008; Shirayama et al., 2004). In turn, these findings raise the possibility that KOR antagonists might be fast-acting and efficacious antidepressants. As such, KOR is a target for development of newer antidepressants. There have been no prior reports of validated PET radiotracers for use in humans to image the KOR, although several tracers have been proposed and validated for MOR (Dannals et al., 1985), for MOR and KOR (Pert et al., 1984), and for DOR (Kinter and Lever, 1995).

GR89696 ((±)-4-[(3,4-dichlorophenyl)acetyl]-3-[(1-pyrrolidinyl)methyl]-1-piperazine carboxylate) is a potent KOR agonist (Naylor et al., 1993). Its ^{11}C-labeled form was evaluated as a PET radiotracer in mice and baboons (Ravert et al., 1999; Talbot et al., 2005). GR103545, which is the active (−)-enantiomer of GR89696, is more potent. In *in vitro* radioligand competition assays using recombinant cells expressing KOR, MOR or DOR, GR103545 was shown to bind to KOR with high affinity (K_i of 0.02 ± 0.01 nmol/L) and excellent selectivity over MOR (K_i of 16 ± 5 nmol/L) and DOR (K_i of 536 ± 234 nmol/L) (Schoultz et al., 2010). In initial *in vivo* evaluations in non-human primates (Schoultz et al.,

2010; Talbot et al., 2005) [^{11}C]GR103545 was shown to have favorable characteristics: excellent brain penetration, significant washout, moderate metabolic rate in the plasma, and good specific binding signals. The uptake pattern of [^{11}C]GR103545 was in good agreement with the known distribution of KOR in the non-human primate brain. The *in vivo* K_D of [^{11}C]GR103545 was estimated from a study in rhesus monkeys and an appropriate tracer mass dose limit was selected for human study (Tomasi et al., 2013). However, its translation to humans was hampered by the absence of an efficient radiosynthetic method. Recently a one-pot method for the automated radiosynthesis of [^{11}C]GR103545 was developed with reliably high specific activity and radiochemical yield (Nabulsi et al., 2011).

Building upon these encouraging preliminary data in non-human primates and the development of an efficient radiosynthesis, we carried out experiments to fully validate [^{11}C]GR103545 as a radiotracer to image and quantify KOR in the human brain. First, a test-retest study was conducted to assess the suitability of kinetic models and the reproducibility of model-derived kinetic parameters. Second, the non-displaceable distribution volume (V_{ND}) was determined from a blocking study with the non-selective opioid antagonist naltrexone. Third, a receptor occupancy study was performed in humans to determine the half maximal inhibitory concentration (IC_{50}) of PF-04455242 (2-methyl-*N*-((2′-(pyrrolidin-1-ylsulfonyl)biphenyl-4-yl)methyl)propan-1-amin), a potent and selective KOR antagonist (K_i of 3 nmol/L for KOR) in development as a novel therapeutic agent for depression (Grimwood et al., 2011).

MATERIALS AND METHODS

Human subjects

Eleven healthy subjects (25–52 years of age; 9 men and 2 women) completed the test-retest part of the study. Seven healthy subjects (26–55 years of age; 4 men and 3 women) were involved in the baseline-blocking study with naltrexone as the blocking drug, while six healthy male subjects (26–51 years of age) were enrolled in the receptor occupancy study with PF-04455242. A total of 24 subjects were enrolled in the study. There were no overlapping subjects among the three parts of the study. The maximum number of scans for any subject was 3. The receptor occupancy study was conducted in compliance with the ethical principles originating in or derived from the Declaration of Helsinki and in compliance with all International Conference on Harmonization (ICH) Good Clinical Practice (GCP) guidelines. In addition, all local regulatory requirements were followed, in particular, those affording greater protection to the safety of trial participants. These studies were performed under protocols approved by the Yale University Human Investigation Committee and the Yale-New Haven Hospital Radiation Safety Committee. Written informed consent was obtained from all subjects. As part of the evaluation procedure, magnetic resonance (MR) images were acquired on all subjects to eliminate those with structural brain abnormalities and for image registration. MR imaging was performed on a 3T whole-body scanner (Trio, Siemens Medical Systems, Erlangen, Germany) with a circularly polarized head coil. The dimension and pixel size of MR images were 256×256×176 and 0.98×0.98×1.0 mm^3, respectively.

Radiotracer synthesis

[^{11}C]GR103545 was synthesized as previously described (Nabulsi et al., 2011). Radiochemical purity of the [^{11}C]GR103545 final product solution was >95%.

Test-retest study

Among the 11 subjects who underwent two 150-min PET scans with [^{11}C]GR103545; 9 of these scan pairs were performed on the same day. The test and retest scans were 6 days apart for one subject and 2 months apart for the other subject. PET scans were performed on the High Resolution Research Tomograph (HRRT) (Siemens Medical Solutions, Knoxville, TN, USA), which acquires 207 slices (1.2 mm slice separation) with a reconstructed image resolution of ~3 mm. Prior to tracer administration, a 6-min transmission scan was conducted for attenuation correction. Each scan was acquired in list mode after intravenous administration of [^{11}C]GR103545 over 1 min by an automatic pump (Harvard PHD 22/2000, Harvard Apparatus, Holliston, MA, USA). The injected mass limit was 0.02 μg/kg body weight (Tomasi et al., 2013). Dynamic scan data were reconstructed in 36 frames (6 × 0.5 min, 3 × 1 min, 2 × 2 min, 22 × 5 min, 3 × 10 min) with corrections for attenuation, normalization, scatter, randoms, and deadtime using the MOLAR algorithm (Carson et al., 2003). Motion correction was included in the reconstruction program based on measurements with the Polaris Vicra sensor (NDI Systems, Waterloo, Canada) with reflectors mounted on a swim cap worn by the subject.

Blocking study with naltrexone

Baseline-blocking experiments were conducted with the non-selective opioid receptor antagonist naltrexone. Subjects underwent two PET scans on the same day: a baseline PET scan followed by a second scan at 75 min after an oral administration of 150 mg naltrexone. For one subject, the blocking scan with naltrexone was conducted 1 month after the baseline scan due to chemistry equipment failure.

Receptor occupancy study with PF-04455242

Subjects received three PET scans with [^{11}C]GR103545 over two days. A baseline scan was obtained on Day 1. On Day 2, the subjects first received a single oral dose of PF-04455242 and then underwent two [^{11}C]GR103545 PET scans, at 1.5 h (post-dose scan #1) and 8 h (post-dose scan #2), respectively, after drug administration. This timing was chosen based on previously acquired human pharmacokinetic data (Sawant Basak et al., 2013). The doses of PF-04455242 were 15 mg (n = 1) and 30 mg (n = 5). Eight venous blood samples were drawn from each subject at 1.5, 2.0, 2.5, 3.0, 4.0, 8.0, 9.0, and 10.5 h following PF-04455242 administration and analyzed to determine the plasma concentration of PF-04455242 over time. The plasma samples were analyzed by LC/MS/MS.

Input function measurement

For each study, the radial artery was cannulated for blood sampling. An automated blood counting system (PBS-101, Veenstra Instruments, Joure, The Netherlands) was used to measure the radioactivity in whole blood during the first 7 min. Fifteen samples (2 to 10 mL) were collected manually at selected time points after tracer administration starting at 3

min. For each sample, plasma was obtained by centrifugation at 4 °C (2930 *g* for 5 min). Whole blood and plasma were counted in cross-calibrated gamma counters (WIZARD 1480 & 2480, PerkinElmer, Waltham, MA, USA).

To determine radioactivity in plasma for the first 7 min, the whole blood-to-plasma ratios were calculated from the hand-drawn samples. The ratios between 3 and 150 min were fitted to the following equation: $a\ t + b$, which was chosen empirically, based on the shape of the curve, and resulting good quality fits of the entire curve of ratios vs. time, and the plasma time-activity curve (TAC) in the first 7 min was calculated from the measured whole blood TAC and the extrapolated ratio. These data were combined with those from the plasma samples to produce the final curve of total radioactivity in plasma. In order to reduce noise in these data, the total plasma curve from ~5 min onward was fitted to a sum of exponentials.

Plasma metabolite analysis

Analysis of the metabolite profile in the arterial plasma was performed using a modified column-switching HPLC method (Hilton et al., 2000). Plasma samples collected at 5, 15, 30, 60, 90, and 120 min after injection were mixed with urea (8 M) and citric acid (32 mg) and then filtered through 0.45 μm syringe filters (Millex-HA, Millipore Corp., Bedford, MA, USA). Up to 5 mL of plasma filtrate was injected to the automatic HPLC system equipped with a Luna C18(2) analytical column (4.6 × 250 mm, 5 μm, Phenomenex, Torrance, CA, USA) and eluted with a mobile phase consisting of 32% acetonitrile and 68% 0.1 M ammonium formate (pH 6.4) at a flow rate of 1.6 mL/min. Retention time for [^{11}C]GR103545 was ~12 min. HPLC eluate was fraction-collected and counted in the gamma counters. The sample recovery rate, extraction efficiency, and HPLC fraction recovery were monitored. The counts of fractions were also corrected for volume and decay. The unmetabolized parent fraction was calculated as the ratio of the sum of radioactivity in fractions containing the parent compound to the total amount of radioactivity collected, and fitted to an integrated gamma function:

$$f(t)=a\times\left(1-b\int_0^{ct}\exp(-u)u^{d-1}\mathrm{d}u/\int_0^{\infty}\exp(-u)u^{d-1}\mathrm{d}u\right) \quad (1)$$

This fraction curve was also corrected for the time-varying extraction efficiency of radioactivity in filtered plasma samples. The fractions were then normalized to the recovery rate, which was determined by a reference plasma sample. The plasma input function was calculated as the product of the total plasma curve and the parent fraction curve.

For three subjects in the receptor occupancy study, only venous, not arterial, samples were available during post-dose scan #2 (at 8 h after oral dose of PF-04455242). In these scans the total arterial plasma radioactivity at post-dose scan #1 was scaled by the injected dose and corrected for the parent fraction in the venous samples measured during post-dose scan #2.

Measurement of tracer free fraction in plasma

Arterial blood samples were taken immediately prior to [^{11}C]GR103545 injection for analysis of plasma free fraction (f_p). An ultrafiltration (Millipore Centrifree® micropartition device, Billerica, MA, USA) method was used for measuring f_p of [^{11}C]GR103545 in plasma in triplicate. The free fraction f_P was determined from the count ratio of ultrafiltrate to plasma.

Image registration and definition of regions of interest

Regions of interest (ROI) were taken from the Automated Anatomical Labeling (AAL) for SPM2 (Tzourio-Mazoyer et al., 2002) in Montreal Neurological Institute (MNI) space (Holmes et al., 1998). For each subject, the dynamic PET images after hardware motion correction were co-registered to the early summed PET images (0 to 10 min post-injection) using a 6-parameter mutual information algorithm (Viola and Wells III, 1997) (FLIRT, FSL) to eliminate any residual motion. Data from one subject in the PF-04455242 receptor occupancy study were excluded due to excessive, uncorrectable motion. The summed PET image was then co-registered to the subject's T1-weighted 3T MR image (6-parameter affine registration), which was subsequently co-registered to the AAL template in MNI space using a nonlinear transformation (Bioimage suite) (Papademetris et al., 2005). Using the combined transformation from template to PET space, regional TACs were generated for 14 ROIs: amygdala, caudate, centrum semiovale, cerebellum, anterior cingulate cortex, posterior cingulate cortex, frontal lobe, globus pallidus, hippocampus, insula, occipital lobe, putamen, temporal lobe, and thalamus.

Quantitative analysis

Outcome measures were derived with kinetic analysis of the regional TACs using the arterial plasma TAC as input function. The distribution volume (V_T) (Innis et al., 2007) was calculated using one- and two-tissue compartment models (1TC, 2TC), as well as the multilinear analysis-1 (MA1) method (Ichise et al., 2002). Due to the lack of a suitable reference region (see below), reference tissue models were not applied. All modeling was performed with in-house programs written with IDL 8.0 (ITT Visual Information Solutions, Boulder, CO, USA). The stability of V_T was assessed by shortening the fitting interval. Scan durations ranging from 60 to 150 min were evaluated. For each region and duration, the ratio of the estimated V_T values to the 150-min values was calculated. The following two criteria were used to select optimal scan duration (Frankle et al., 2004): (a) the average of this ratio was between 0.95 and 1.05; and (b) the inter-subject standard deviation of this ratio was italic> 0.1.

For the descriptive analysis of the test-retest data, results were evaluated according to three criteria: relative test-retest variability (TRV), absolute test-retest variability (aTRV), and intra-class correlation coefficient (ICC). TRV is calculated as follows:

$$\mathrm{TRV}=\frac{p_{\mathrm{test}}-p_{\mathrm{retest}}}{(p_{\mathrm{test}}+p_{\mathrm{retest}})/2} \quad (2)$$

where p_{test} and p_{retest} indicate the parameter p measured at the test and retest scans, respectively. The mean of TRV indicates a presence of a trend between the two scans, and the standard deviation of TRV is an index of the variability of the % difference of two estimates. aTRV was calculated as the absolute value of TRV and mean of aTRV combines these two effects; in the absence of between-scan trend, aTRV is comparable to the % error in a single measurement. To evaluate the within-subject variability relative to the between-subject variability, the ICC was computed using the following equation:

$$\mathrm{ICC}=\frac{\mathrm{BSMSS}-\mathrm{WSMSS}}{\mathrm{BSMSS}+(k-1)\mathrm{WSMSS}} \quad (3)$$

where BSMSS is the mean sum of squares between subjects, WSMSS is the mean sum of squares within subjects, and k is the number of repeated observations (k = 2 for test-retest protocol). The value of ICC ranges from -1 (no reliability, BSMSS = 0) to 1 (identity between test and retest, WSMSS = 0) (Frankle et al., 2006; Ogden et al., 2007).

KOR occupancy (r) and non-displaceable distribution volume (V_{ND}) were calculated from the following equation (Cunningham et al., 2010):

$$V_T(\mathrm{baseline})-V_T(\mathrm{blocking})=r(V_T(\mathrm{baseline})-V_{ND}) \quad (4)$$

For each subject, the percentage specific binding was calculated as the difference between V_T and V_{ND} divided by V_T. For the receptor occupancy study with PF-04455242, two occupancy plots at 1.5 h and 8 h after administration of PF-04455242 were fitted simultaneously with a common V_{ND} using nonlinear regression (Levenberg-Marquardt method). All regions were used for the occupancy plots in the naltrexone blocking study, while the amygdala was excluded from the plots for the PF-04455242 receptor occupancy study because its V_T had large % standard errors (%SE).

To characterize the relationship between PF-04455242 pharmacokinetic (PK) concentration (C) and r, an average total PF-04455242 concentration in the venous plasma was calculated during each scan for each subject, and the single-site occupancy model ($C/(C+IC_{50})$) was applied to estimate the IC_{50} value (the concentration to achieve 50% of the maximum r). Occupancy plots and PK/RO E_{max} modeling were calculated using GraphPad Prism 5 software (GraphPad Software, Inc., La Jolla, CA, USA).

Statistical methods

Values are given as mean ± standard deviation. Goodness-of-fit was evaluated by visual inspection and by calculating the Akaike information criterion (AIC) (Akaike, 1974) and the F test using the weighted residual sum of squares. Statistical significance using the F test was assessed with P bold> 0.05.

Results

Injection parameters

Injection parameters are listed in Table 1. For the test-retest portion of study, subjects received radioactivity dose of 504 ± 170 MBq (range of 171 to 730 MBq) with specific activity of 189 ± 86 GBq/μmol (range of 50 to 398 GBq/μmol) at the time of injection. The injected dose and injected mass did not significantly differ between the test and retest scans (P = 0.70 and 0.46, respectively, paired t-test, Table 1). For the baseline and blocking study with naltrexone, subjects received 390 ± 216 MBq (range of 57 to 749 MBq) of [^{11}C]GR103545 with specific activity of 375 ± 136 GBq/μmol (range of 178 to 659 GBq/μmol) at the time of injection. Subject enrolled in the PF-04455242 occupancy study received a radioactivity dose of 463 ± 224 MBq (range of 89 to 742 MBq) with specific activity of 149 ± 78 GBq/μmol (range of 25 to 291 GBq/μmol) at the time of injection. For all subjects, injected mass was controlled at ≤ 0.02 μg/kg via a computer-controlled pump to maintain tracer level.

Plasma analysis

In either the baseline or blocking scan, total plasma activity stabilized at a constant level after 20 min post-injection (Figures 1A and 2A). The parent fraction did not significantly differ between the test and retest scans. The parent fractions for the test-retest and all other baseline scans (n = 35) were 67% ± 8% and 38% ± 7% at 30 and 90 min post-injection, respectively (Figure 1B). The parent fraction in the blocking scans (either with naltrexone or with PF-04455242) was similar to that from the baseline scans (Figure 2B). The difference in the parent fraction in the arterial plasma at baseline scan and that in venous plasma at post-dose scan #2 was not significant (2% ± 5%). The estimated metabolite-corrected radioactivity in the arterial plasma is shown in Figures 1C and 2C. The plasma free fraction (f_P) of [^{11}C]GR103545 was 0.20 ± 0.04 for test-retest and other baseline scans (n = 35) and 0.22 ± 0.06 for blocking scans (n = 19). The TRV of f_P was -4% ± 10%, with no significant change between the test and retest scans (P = 0.21, paired t-test), or between baseline and blocking scans (P = 0.16, paired t-test).

Brain uptake

Uptake images from the test-retest and test-blocking protocols are shown in Figure 3. TACs for representative brain regions are shown in Figure 4. In the regions with high or intermediate uptakes, such as insula, putamen, frontal cortex, and occipital cortex, uptake reached plateau at ~100 min. Activity peaked earlier (~30 min) in the low uptake regions (cerebellum and thalamus).

Kinetic model assessment

The test-retest scans were chosen to assess the best model for kinetic analysis. The 1TC and 2TC models reached convergence for every scan in all regions. The mean value of K_1 in the 1TC model ranged from 0.06 mL/cm^3/min in the centrum semiovale to 0.14 mL/cm^3/min in the occipital cortex.

The 2TC model was favored over the 1TC model in terms of the AIC and visual assessment of the quality of fits. The *F* test indicated a significantly better fit for the 2TC model in 291 out of 308 regions. However, the 2TC model provided implausibly large V_T estimates (k_4 < 0.01 min^{-1}, V_T > 100 mL/cm^3), with large %SE, most often found in the high uptake regions. Due to the lack of fit with 1TC model and the variability of 2TC V_T estimates, the MA1 model was evaluated. While the V_T values using the 1TC model were lower than those using the 2TC model ($V_{T\ (1TC)} = 0.75\ V_{T\ (2TC)} + 1.26$, $R^2 = 0.94$), the V_T values from MA1 (t^*=40 min) matched well with those from the 2TC model ($V_{T\ (MA1,\ t^*=40\ min)} = 0.98\ V_{T\ (2TC)} + 0.19$, $R^2 = 0.96$). Note that this comparison was conducted for the regions with good identifiability, i.e., %SE of V_T < 10% with the 2TC model (229 out of 308 regions). The results from MA1 model are shown in Table 2. High V_T values were seen in the amygdala, anterior cingulate cortex, and insula. Intermediate V_T values were found in the temporal cortex, frontal cortex, globus pallidus, and putamen. Low V_T values were observed in the occipital cortex, caudate, hippocampus, posterior cingulate cortex, cerebellum and centrum semiovale, with the lowest V_T value in the thalamus.

TACs were fitted for different scan durations with MA1 analysis, to define the minimum scan time required for reliable estimates of V_T (Table 2). Using comparatively strict criteria, minimal scanning time ranged from 70 to 140 min. The shortest and longest minimum scan durations applied to the thalamus and amygdala, respectively, the regions with the lowest and highest V_T values.

Test-retest variability and reproducibility of binding parameters

Table 3 summarizes the results of test-retest variability and reproducibility assessment using MA1. For each criterion, the mean was calculated across all regions except for the amygdala. Global mean TRV was 5% and 9% for V_T and V_T/f_P. Global mean aTRV was 13% and 16% for V_T and V_T/f_P, respectively. ICC was 0.81 ± 0.08 for V_T and 0.69 ± 0.11 for V_T/f_P. Showing a divergence from other regions, the amygdala displayed a large TRV (V_T: 41%, V_T/f_P: 41%) and low ICC (V_T: 0.05, V_T/f_P: 0.11).

Blocking of specific binding by naltrexone

Naltrexone induced a significant reduction in regional V_T as seen in Figures 3D and 4C and Table 4. The non-displaceable distribution volume (V_{ND}) and KOR occupancy for [^{11}C]GR103545 was estimated as 3.4 ± 0.9 mL/cm^3 (range: 2.1 to 5.0 mL/cm^3) and 85 ± 10 % (range: 72 to 97 %), respectively, from occupancy plots of the blocking experiments with naltrexone. Based on the reduction of binding by naltrexone, the specific binding percentage ($(V_T\text{-}V_{ND})/V_T$) in the thalamus, a region with the lowest V_T, was estimated at 56 ± 8% (range of 39% to 63%). Using this V_{ND} value, the range of regional non-displaceable binding potential (BP_{ND}) ranged from 1.1 (thalamus) to 7.4 (amygdala), as derived from the equation $BP_{ND} = (V_T\text{-}V_{ND})/V_{ND}$ (Innis et al., 2007).

Receptor occupancy by PF-04455242

Occupancy values of 45 ± 6 % and 24 ± 4 % were observed at 1.5 and 8 h after 30 mg oral dose of PF-04455242, respectively. Figure 5 shows an example of the occupancy plots where the 2 post-dose datasets were fitted with a common V_{ND} value. Occupancies after a

15 mg dose of PF-04455242 (27 % at 1.5 h and 5% at 8 h) were lower than those from the 30 mg dose. While the slope of the individual occupancy plot was significant for all but one case (estimated 5% occupancy), in all cases the slopes of dual fitting method with a common V_{ND} value were shown to be significantly different from zero. Even with the dual fitting method, there was substantial intersubject variability in the non-displaceable distribution volume, V_{ND} (2.1 ± 1.3 mL/cm^3); this is not surprising since V_{ND} cannot be reliably estimated in cases of low occupancy. There was a significant reduction in thalamus V_T from baseline to post-dose scan #1 (P = 0.001, n = 5), but no significant difference was seen between the baseline scan and post-dose scan #2 (P = 0.07, n = 5).

KOR occupancy (r) measured by PET was plotted against the average total PF-04455242 plasma concentrations and modeled to further quantify the PK concentration-RO relationship. Due to the limited data at high r values, a 2-parameter fit of the maximum occupancy (E_{max}) and IC_{50} could not be confidently estimated. E_{max} was therefore fixed to 100% in order to estimate IC_{50} value, at 55.3 ± 4.9 ng/mL. A previous analysis using slightly different methods reported an IC_{50} of 48.6 ± 7.2 ng/mL (Jacobsen et al., 2010). Figure 6 shows the relationship between observed average PF-04455242 plasma concentration and KOR r, the mean prediction by the model. Individual subjects are plotted with different symbols.

Comparison of in vivo and in vitro affinity of [^{11}C]GR103545

Regional distribution of μ, δ and κ opioid receptors in human has previously been studied in radioligand completion assays with homogenized brain tissue or autoradiography and the radioligand [^{3}H]diprenorphine (Pfeiffer et al., 1982), [^{3}H]etrophine (Cross et al., 1987; Delay-Goyet et al., 1987), or [^{3}H]ethylketocyclazocine (Delay-Goyet et al., 1987) in the presence of different displacing agents or [^{3}H]U69593 (Barg et al., 1993). We took the regional KOR concentrations (B_{max}) from these reports and calculated the unweighted averages as presented in Table 5. Note that *in vitro* B_{max} in the regions of amygdala, putamen, and globus pallidus measured by [^{3}H]etorphine were excluded from the average (see below). In the *in vitro* literature, the unit of specific binding is fmol/mg protein. The unit can be converted to fmol/mg of wet tissue by assuming that 1 fmol/mg protein is approximated by 0.1 fmol/mg of wet tissue (Laruelle et al., 1988). The data from Table 5 were correlated with the *in vivo* receptor measures derived from the present study to estimate the *in vivo* binding affinity (K_D) of [^{11}C]GR103545.

Assuming a mean V_{ND} of 3.4 mL/cm^3 as determined from the occupancy plots of naltrexone, and a mean plasma free fraction of 0.20 for [^{11}C]GR103545, free fraction in the nondisplaceable compartment (f_{ND}) was determined to be 0.059, according to the equation, $f_{ND} = f_P/V_{ND}$ (Innis et al., 2007). A correlation plot of the regional binding potential BP_F (= $(V_T\text{-}V_{ND})/f_P = B_{avail}/K_D$) and the *in vitro* B_{max} estimates from Table 5 was thus generated and shown in Figure 7, by plotting BP_F against B_{max}. A good correlation was found with the regression equation of $B_{max} = 0.069 \times BP_F$ (R^2 = 0.51, $P < 0.0001$, n = 10). The slope of this regression line represented the estimate of *in vivo* K_D for [^{11}C]GR103545. The *in vivo* K_D values are in excellent agreement with the inhibition coefficient (K_i) of 0.02 nmol/L measured *in vitro* (Schoultz et al., 2010) using cloned human KOR, and the *in vivo* K_D

estimate of 0.048 nmol/L derived from [^{11}C]GR103545 PET imaging study in rhesus monkey (Tomasi et al., 2013). The relationship between BP_F and *in vitro* B_{max} was also evaluated using B_{max} values from individual studies. From that analysis, the estimated K_D values ranged from 0.047 nmol/L ([^{3}H]diprenorphine) to 0.11 nmol/L ([^{3}H]etrophine by Cross et al, 1987 and [^{3}H]U69593). The individual correlation plots were shown in Supplemental figure 1. In the analysis, *in vitro* B_{max} in the regions of amygdala, putamen, and globus pallidus measured by [^{3}H]etorphine were low and determination coefficient was very low ($R^2 < 0.1$). Thus the three regions were excluded from the comparison.

Discussion

This is the first human study with the potent and selective KOR agonist tracer [^{11}C]GR103545 to evaluate its ability to image KOR and accurately estimate regional binding parameters in the human brain. In addition, the receptor occupancy by naltrexone and a selective KOR antagonist were also evaluated. Thus, we consider this to be a comprehensive first evaluation of this tracer.

[^{11}C]GR103545 displays a moderate rate of metabolism in human and a relatively high plasma free fraction. [^{11}C]GR103545 has been studied previously in awake monkey (Schoultz et al., 2010) and anesthetized baboon (Talbot et al., 2005). Compared to these studies, metabolism of [^{11}C]GR103545 was slower in human, with parent fractions of 67% and 47% at 30 and 60 min post injection, vs. 49% and 35% in rhesus monkey, and 35% and 25% in baboon, respectively (Schoultz et al., 2010; Talbot et al., 2005). Plasma free fraction was similar among human, monkey, and baboon (20% in human, 22% in monkey, and 24% in baboon).

In the human brain [^{11}C]GR103545 displayed high uptake, with peak SUV of 2.4 in the thalamus to 3.5 in the amygdala. Levels of regional uptake in human were similar to those in rhesus monkey and baboon. However, the tissue kinetic in the human brain was slow (e.g., K_1 = ~0.1 mL/cm^3/min), and hence slow to reach equilibrium. In most brain regions, uptake of [^{11}C]GR103545 either continued to rise or plateaued at ~100 min during the 150 min scan, with only cerebellum and thalamus showing a peak at ~30 min (Fig. 4A and 4B). Results from nonhuman primates and the present study in humans indicate that [^{11}C]GR103545 displays a slower washout from brain tissue in monkey and human than baboon. The peak time of regional TACs was similar in awake monkey (peak time of ~1 h) and human (peak time of ~1.5 h). Regional TACs in baboon display an earlier peak time (16 ± 3 min, n = 4). The faster kinetics of [^{11}C]GR103545 in baboon might be attributed, at least in part, to its faster metabolism rate in this species (see above).

In non-human primate studies, the 2TC model was chosen as the method of choice for the analysis of TACs and derivation of kinetic parameters (Schoultz et al., 2010; Talbot et al., 2005). Similarly, the 2TC model provided a better fit in all regions than the 1TC model in humans. However, it was observed that in high binding regions the 2TC model produced high V_T estimates with large standard errors. The unreliability of V_T values in these regions was due to the slow washout of the tracer from the brain, which made it difficult to estimate microparameters k_2, k_3, and k_4, leading to high variability of V_T values. Given that V_T

estimates from MA1 were in good agreement with those derived from the 2TC model and were associated with a small standard error, MA1 was considered as the method of choice for kinetic analysis in human. MA1 analysis yielded stable V_T estimates in terms of bias and variance for acquisitions of 120 min or shorter, except for the amygdala. Since a stable estimate of V_T could not be obtained for the highest binding regions until 100 min or later, we cannot rule out the possibility of underestimation of V_T for these regions in the baseline scans, due to the tracer's slow kinetics, which would lead to the underestimation of receptor occupancy.

Test-retest variability of MA1 derived V_T estimates was fair across all the regions (aTRV of 8–17%) except for the amygdala and anterior cingulate cortex, which showed absolute TRV of 41% and 19%, respectively (Table 3). Test-retest reproducibility of V_T estimates, as measured by ICC was also generally good (0.67 to 0.92), with the exception of the amygdala (ICC = 0.05) (Table 3). With these TRV values, [^{11}C]GR103545 may not be as useful as some tracers for other targets for determination of between-group differences in receptor availability in high binding regions, but adequate for other, lower binding regions. Given the slow kinetics of this ^{11}C-labeled tracer, due largely to its high KOR affinity, one way to improve the reliability of binding parameter estimates would be to develop an ^{18}F-labeled version of the agonist tracer to allow for longer scan time to capture equilibrium. Another way might be to develop a new ^{11}C-labeled tracer with lower affinity and thus faster kinetics. Both of these approaches are being pursued in our laboratory. However [^{11}C]GR103545 should be suitable for use in receptor occupancy studies which target high occupancy (>50%) and use data from many regions. In the present study, the PF-04455242 dose was not raised to target higher KOR occupancy, as the study was terminated due to preclinical toxicology findings. In the blocking study with 150 mg of oral naltrexone, high occupancy (85 ± 10%) was reliably measured with [^{11}C]GR103545, proving the usefulness of the tracer in occupancy studies.

The plasma free fraction (f_P) was measured in this study, allowing for correction of V_T values. This correction is useful if f_P can be measured reliably and if there is substantial intersubject variation. However, the TRV and absolute TRV were higher and ICC was lower for V_T/f_P compared to V_T. Hence, the normalization of V_T by f_P did not reduce variability in this case.

A previous baboon study using naloxone as a blocking agent indicated that the cerebellum was a suitable reference region, as V_T in the region remained unchanged under the blocking conditions (Talbot et al., 2005). In the human study, however, it was the thalamus, not the cerebellum, that had the lowest V_T. Further, V_T decreased in all regions when the subjects were treated either with the non-selective opioid antagonist naltrexone or the selective KOR antagonist PF-04455242. Naltrexone at a dose of 150 mg produced sufficient blocking of specific binding to allow for a reliable estimate of V_{ND}. Based on this V_{ND} value, the non-specific binding component was estimated to account for more than half of the V_T in the thalamus, a region with the lowest uptake. Thus, we found no suitable reference region for [^{11}C]GR103545 in human. Therefore, derivation of receptor binding parameters requires acquisition of an arterial input function.

Comparing *in vivo* studies in non-human primates (Schoultz et al., 2010; Talbot et al., 2005; Tomasi et al., 2013) and humans with [^{11}C]GR103545, differences were seen in the rank order of V_T. In the non-human primate studies, cingulate cortex and striatum showed the highest binding, followed by insula, neocortical regions, thalamus, amygdala, and lowest in the cerebellum. In contrast, in the human brain the amygdala displayed the highest uptake, and thalamus the lowest. Uptake in the striatum was lower than those in neocortical regions. *In vitro* autoradiography studies have indicated a similar distribution of KOR in non-human primates and humans. However, an interesting species difference in KOR distribution was observed in this first *in vivo* investigation of KOR using the agonist radiotracer [^{11}C]GR103545. Since an agonist radiotracer labels only the portion of receptors configured in the high-affinity state, it is not clear whether this discrepancy observed with [^{11}C]GR103545 reflects a true difference in total KOR population, or receptor affinity state between the species. Nonetheless, it is an intriguing question to be answered with a KOR antagonist tracer that can be used to measure the total KOR expression in the human brain region. We are currently conducting a study in this regard.

KOR distribution in the human brain has been investigated by sequential displacement of [^{3}H]diprenorphine (Pfeiffer et al., 1982), [^{3}H]etorphine (Cross et al., 1987; Delay-Goyet et al., 1987), or [^{3}H]ethylketocyclazocine (Delay-Goyet et al., 1987) bindings at the μ-, δ-, and κ-sites and by [^{3}H]U69593 binding (Barg et al., 1993). Regional BP_F values derived from the present study showed a good correlation with the regional composite B_{max}. From this correlation study, the *in vivo* binding affinity (*in vivo* K_D) of [^{11}C]GR103545 was estimated to be 0.069 nmol/L, a value in excellent agreement with the K_i of GR103545 measured *in vitro* and the *in vivo* K_D measured in the brain of rhesus monkey. *In vivo* K_D values estimated using B_{max} from individual *in vitro* study ranged from 0.047 to 0.11 nmol/L. The variation in *in vivo* K_D estimates result from the discrepancies in regional B_{max} among the studies using different radioligands.

We evaluated the KOR occupancy of PF-04455242 by comparing two post-dose scans to the baseline scan. Since V_{ND} could not be reliably estimated from the low occupancy in the 8 h post-dose scans, we evaluated a paired fitting method, where the V_{ND} estimate was shared for the 2 post-dose scans. Note that this simultaneous fitting approach provided similar estimates of occupancy to those obtained from separate fitting. It is worth noting that data points taken at 1.5 and 8 h post-dose for each subject had a consistent relationship with respect to the mean PK-RO curve. This suggests the absence of a substantial delay (or hysteresis) in the exchange of PF-04455242 across the blood-brain barrier. In the presence of significantly delayed transit across the blood-brain barrier, PK at t_{max} would be inconsistent with the occupancy at t_{max} since the brain and blood would not be at equilibrium; in this case, a more complex model to compare RO and PK would be required (Abanades et al., 2011).

A translational pharmacokinetic-pharmacodynamic (PK-PD) study was performed previously with PF-04455242 to estimate its K_i in rats and humans and a competitive antagonism model was used to describe the effect of PF-04455242 on prolactin release stimulated by the KOR agonist spiradoline (Chang et al., 2011). The PK-PD model-based estimate of K_i for PF-04455242 in rats was 414 ng/mL, which, after accounting for species

differences in plasma free fraction (f_P), translated into a human K_i of 44.4 ng/mL. The human K_i estimate from the clinical spiradoline challenge study was 39.2 ng/mL, which is very close to the current IC_{50} estimate of 55.3 ng/mL from the PF-04455242 PK/RO relationship study using PET imaging with [^{11}C]GR103545.

The estimated KOR IC_{50} values of PF-04455242 from both translational PK-PD modeling (Chang et al., 2011) and PET PK/RO study agree well with the corresponding values from animal models relating PF-04455242 plasma concentration and indication of antidepressant activity (Grimwood et al., 2011). Although RO and suppression of spiradoline-stimulated prolactin release cannot be taken as proxies for antidepressant efficacy in the clinic, these results align closely with preclinical data showing that efficacy in rodent models of depression corresponds to ~50% KOR occupancy (Grimwood et al., 2011). It remains to be proven whether 50% KOR occupancy is associated with antidepressant efficacy in humans, because clinical trials with PF-04455242 were terminated due to preclinical toxicology findings associated with chronic dosing. Nonetheless, these results provide support for testing the KOR antagonist mechanism of antidepressant activity in the clinic, as these levels of target engagement and drug exposure appear to induce an observable effect on a relevant mechanistic biomarker, i.e., suppression of spiradoline-induced plasma prolactin increase(Chang et al., 2011).

Conclusions

[^{11}C]GR103545 can be used for quantitative PET measurement of KOR in the human brain, although it has slow kinetics, and variability of outcome measures is higher than desirable. The distribution volumes can be reliably estimated using the MA1 method with arterial input function. The reduction in uptake in all brain regions by naltrexone suggests that there is no available reference region for this radiotracer, and hence the requirement of an arterial input function for the derivation of kinetic parameters. In addition, [^{11}C]GR103545 has been successfully used in a receptor occupancy study relating the dose and plasma concentration of the KOR antagonist PF-04455242 with receptor occupancy. The calculated IC_{50} value aligns well with preclinical and clinical data. Together with preclinical indication of antidepressant-like activity and clinical evidence of observable antagonist activity at ~50% KOR occupancy, the present PET PK/RO data with PF-04455242 provide support for the notion of KOR antagonism as a potential treatment strategy for depression.

Supplementary Material

Refer to Web version on PubMed Central for supplementary material.

Acknowledgments

The authors appreciate the excellent technical assistance of the staff at the Yale University PET Center and the New Haven Pfizer Clinical Research Unit. We would also like to thank Diana Martinez of Columbia University for providing the human dosimetry data of [^{11}C]GR103545. This study was supported by the Yale-Pfizer Bioimaging Alliance, and by a research grant from NIMH (1 R01 MH091537 to Y. Huang). This publication was also made possible by CTSA Grant UL1 RR024139 from the National Center for Research Resources (NCRR) and the National Center for Advancing Translational Sciences (NCATS), components of the National Institutes of Health (NIH). Its contents are solely the responsibility of the authors and do not necessarily represent the official view of NIH.

Abbreviations

KOR	kappa opioid receptor
MOR	mu opioid receptor
DOR	delta opioid receptor
TRV	relative test-retest variability
aTRV	absolute test-retest variability
ICC	intra-class correlation coefficient

References

Abanades S, van der Aart J, Barletta JA, Marzano C, Searle GE, Salinas CA, Ahmad JJ, Reiley RR, Pampols-Maso S, Zamuner S, Cunningham VJ, Rabiner EA, Laruelle MA, Gunn RN. Prediction of repeat-dose occupancy from single-dose data: characterisation of the relationship between plasma pharmacokinetics and brain target occupancy. Journal of Cerebral Blood Flow and Metabolism. 2011; 31:944–952. [PubMed: 20940733]

Akaike H. New Look at Statistical-Model Identification. IEEE Transactions on Automatic Control Ac19. 1974:716–723.

Barber A, Gottschlich R. Novel developments with selective, non-peptidic kappa-opioid receptor agonists. Expert Opin Investig Drugs. 1997; 6:1351–1368.

Barg J, Belcheva M, Rowinski J, Ho A, Burke WJ, Chung HD, Schmidt CA, Coscia CJ. Opioid receptor density changes in Alzheimer amygdala and putamen. Brain Research. 1993; 632:209–215. [PubMed: 8149229]

Beardsley PM, Howard JL, Shelton KL, Carroll FI. Differential effects of the novel kappa opioid receptor antagonist, JDTic, on reinstatement of cocaine-seeking induced by footshock stressors vs cocaine primes and its antidepressant-like effects in rats. Psychopharmacology. 2005; 183:118–126. [PubMed: 16184376]

Carlezon WA Jr, Beguin C, DiNieri JA, Baumann MH, Richards MR, Todtenkopf MS, Rothman RB, Ma Z, Lee DY, Cohen BM. Depressive-like effects of the kappa-opioid receptor agonist salvinorin A on behavior and neurochemistry in rats. Journal of Pharmacology and Experimental Therapeutics. 2006; 316:440–447. [PubMed: 16223871]

Carson RE, Barker WC, Liow JS, Johnson CA. Design of a motion-compensation OSEM list-mode algorithm for resolution-recovery reconstruction for the HRRT. IEEE 2003 Nuclear Science Symposium Conference Record. 2003; 5:3281–3285.

Chang C, Byon W, Lu Y, Jacobsen LK, Badura LL, Sawant-Basak A, Miller E, Liu J, Grimwood S, Wang EQ, Maurer TS. Quantitative PK-PD model-based translational pharmacology of a novel kappa opioid receptor antagonist between rats and humans. AAPS J. 2011; 13:565–575. [PubMed: 21847689]

Corbett AD, Henderson G, McKnight AT, Paterson SJ. 75 years of opioid research: the exciting but vain quest for the Holy Grail. British Journal of Pharmacology. 2006; 147(Suppl 1):S153–162. [PubMed: 16402099]

Cross AJ, Hille C, Slater P. Subtraction autoradiography of opiate receptor subtypes in human brain. Brain Research. 1987; 418:343–348. [PubMed: 2823963]

Cunningham VJ, Rabiner EA, Slifstein M, Laruelle M, Gunn RN. Measuring drug occupancy in the absence of a reference region: the Lassen plot re-visited. Journal of Cerebral Blood Flow and Metabolism. 2010; 30:46–50. [PubMed: 19738632]

Dannals RF, Ravert HT, Frost JJ, Wilson AA, Burns HD, Wagner HN Jr. Radiosynthesis of an opiate receptor binding radiotracer: [^{11}C]carfentanil. International Journal of Applied Radiation and Isotopes. 1985; 36:303–306. [PubMed: 2991142]

de Lanerolle NC, Williamson A, Meredith C, Kim JH, Tabuteau H, Spencer DD, Brines ML. Dynorphin and the kappa 1 ligand [^{3}H]U69,593 binding in the human epileptogenic hippocampus. Epilepsy Research. 1997; 28:189–205. [PubMed: 9332884]

Delay-Goyet P, Zajac JM, Javoy-Agid F, Agid Y, Roques BP. Regional distribution of mu, delta and kappa opioid receptors in human brains from controls and parkinsonian subjects. Brain Research. 1987; 414:8–14. [PubMed: 3040166]

Frankle WG, Huang Y, Hwang DR, Talbot PS, Slifstein M, Van Heertum R, Abi-Dargham A, Laruelle M. Comparative evaluation of serotonin transporter radioligands ^{11}C-DASB and ^{11}C-McN 5652 in healthy humans. Journal of Nuclear Medicine. 2004; 45:682–694. [PubMed: 15073266]

Frankle WG, Slifstein M, Gunn RN, Huang Y, Hwang DR, Darr EA, Narendran R, Abi-Dargham A, Laruelle M. Estimation of serotonin transporter parameters with ^{11}C-DASB in healthy humans: reproducibility and comparison of methods. Journal of Nuclear Medicine. 2006; 47:815–826. [PubMed: 16644752]

Gerra G, Fantoma A, Zaimovic A. Naltrexone and buprenorphine combination in the treatment of opioid dependence. J Psychopharmacol. 2006; 20:806–814. [PubMed: 16401652]

Grimwood S, Lu Y, Schmidt AW, Vanase-Frawley MA, Sawant-Basak A, Miller E, McLean S, Freeman J, Wong S, McLaughlin JP, Verhoest PR. Pharmacological characterization of 2-methyl-N-((2′-(pyrrolidin-1-ylsulfonyl)biphenyl-4-yl)methyl)propan-1-amine (PF-04455242), a high-affinity antagonist selective for kappa-opioid receptors. Journal of Pharmacology and Experimental Therapeutics. 2011; 339:555–566. [PubMed: 21821697]

Hilton J, Yokoi F, Dannals RF, Ravert HT, Szabo Z, Wong DF. Column-switching HPLC for the analysis of plasma in PET imaging studies. Nuclear Medicine and Biology. 2000; 27:627–630. [PubMed: 11056380]

Holmes CJ, Hoge R, Collins L, Woods R, Toga AW, Evans AC. Enhancement of MR images using registration for signal averaging. Journal of Computer Assisted Tomography. 1998; 22:324–333. [PubMed: 9530404]

Ichise M, Toyama H, Innis RB, Carson RE. Strategies to improve neuroreceptor parameter estimation by linear regression analysis. Journal of Cerebral Blood Flow and Metabolism. 2002; 22:1271–1281. [PubMed: 12368666]

Innis RB, Cunningham VJ, Delforge J, Fujita M, Gjedde A, Gunn RN, Holden J, Houle S, Huang SC, Ichise M, Iida H, Ito H, Kimura Y, Koeppe RA, Knudsen GM, Knuuti J, Lammertsma AA, Laruelle M, Logan J, Maguire RP, Mintun MA, Morris ED, Parsey R, Price JC, Slifstein M, Sossi V, Suhara T, Votaw JR, Wong DF, Carson RE. Consensus nomenclature for in vivo imaging of reversibly binding radioligands. Journal of Cerebral Blood Flow and Metabolism. 2007; 27:1533–1539. [PubMed: 17519979]

Jacobsen, L.; Banerjee, A.; Byon, W.; Huang, Y.; Carson, R.; Tomasi, G.; Weinzimmer, D.; Williams, W.; Lin, S.; Ropchan, J.; McCarthy, T.; Grimwood, S.; Badura, L. Central receptor occupancy and pharmacodynamic action of PF-04455242, a high affinity, selective kappa opioid receptor antagonist, in humans. The 40th Society for Neuroscience Annual Meeting; San Diego, CA. 2010. p. 472.5(abstract)

Kinter CM, Lever JR. Synthesis of radioiodinated naltrindole analogues: ligands for studies of delta opioid receptors. Nuclear Medicine and Biology. 1995; 22:599–606. [PubMed: 7581169]

Laruelle M, Vanisberg MA, Maloteaux JM. Regional and subcellular localization in human brain of [^{3}H]paroxetine binding, a marker of serotonin uptake sites. Biological Psychiatry. 1988; 24:299–309. [PubMed: 2969755]

Loacker S, Sayyah M, Wittmann W, Herzog H, Schwarzer C. Endogenous dynorphin in epileptogenesis and epilepsy: anticonvulsant net effect via kappa opioid receptors. Brain. 2007; 130:1017–1028. [PubMed: 17347252]

Mague SD, Pliakas AM, Todtenkopf MS, Tomasiewicz HC, Zhang Y, Stevens WC Jr, Jones RM, Portoghese PS, Carlezon WA Jr. Antidepressant-like effects of kappa-opioid receptor antagonists in the forced swim test in rats. Journal of Pharmacology and Experimental Therapeutics. 2003; 305:323–330. [PubMed: 12649385]

Mash DC, Staley JK. D_3 dopamine and kappa opioid receptor alterations in human brain of cocaine-overdose victims. Annals of the New York Academy of Sciences. 1999; 877:507–522. [PubMed: 10415668]

Mathieu-Kia AM, Fan LQ, Kreek MJ, Simon EJ, Hiller JM. Mu-, deltaand kappa-opioid receptor populations are differentially altered in distinct areas of postmortem brains of Alzheimer's disease patients. Brain Research. 2001; 893:121–134. [PubMed: 11223000]

McLaughlin JP, Marton-Popovici M, Chavkin C. Kappa opioid receptor antagonism and prodynorphin gene disruption block stress-induced behavioral responses. Journal of Neuroscience. 2003; 23:5674–5683. [PubMed: 12843270]

Mello NK, Negus SS. Interactions between kappa opioid agonists and cocaine. Preclinical studies. Annals of the New York Academy of Sciences. 2000; 909:104–132. [PubMed: 10911926]

Nabulsi NB, Zheng MQ, Ropchan J, Labaree D, Ding YS, Blumberg L, Huang Y. [^{11}C]GR103545: novel one-pot radiosynthesis with high specific activity. Nuclear Medicine and Biology. 2011; 38:215–221. [PubMed: 21315277]

Naylor A, Judd DB, Lloyd JE, Scopes DI, Hayes AG, Birch PJ. A potent new class of kappa-receptor agonist: 4-substituted 1-(arylacetyl)-2- [(dialkylamino)methyl]piperazines. Journal of Medicinal Chemistry. 1993; 36:2075–2083. [PubMed: 8393489]

Newton SS, Thome J, Wallace TL, Shirayama Y, Schlesinger L, Sakai N, Chen J, Neve R, Nestler EJ, Duman RS. Inhibition of cAMP response element-binding protein or dynorphin in the nucleus accumbens produces an antidepressant-like effect. Journal of Neuroscience. 2002; 22:10883–10890. [PubMed: 12486182]

Ogden RT, Ojha A, Erlandsson K, Oquendo MA, Mann JJ, Parsey RV. In vivo quantification of serotonin transporters using [^{11}C]DASB and positron emission tomography in humans: modeling considerations. Journal of Cerebral Blood Flow and Metabolism. 2007; 27:205–217. [PubMed: 16736050]

Papademetris X, Jackowski M, Rajeevan N, Constable RT, Staib LH. Bioimage suite: An integrated medical image analysis suite. The Insight Journal - 2005 MICCAI Open-Source Workshop. 2005

Pert CB, Danks JA, Channing MA, Eckelman WC, Larson SM, Bennett JM, Burke TR Jr, Rice KC. 3-[^{18}F]Acetylcyclofoxy: a useful probe for the visualization of opiate receptors in living animals. FEBS Letters. 1984; 177:281–286. [PubMed: 6094248]

Pfeiffer A, Pasi A, Mehraein P, Herz A. Opiate receptor binding sites in human brain. Brain Research. 1982; 248:87–96. [PubMed: 6289997]

Ravert HT, Mathews WB, Musachio JL, Scheffel U, Finley P, Dannals RF. [^{11}C]-methyl 4-[(3,4-dichlorophenyl)acetyl]-3-[(1-pyrrolidinyl)-methyl]-1-piperazinecarboxylate ([^{11}C]GR89696): synthesis and in vivo binding to kappa opiate receptors. Nuclear Medicine and Biology. 1999; 26:737–741. [PubMed: 10628552]

Reindl JD, Rowan K, Carey AN, Peng X, Neumeyer JL, McLaughlin JP. Antidepressant-like effects of the novel kappa opioid antagonist MCL-144B in the forced-swim test. Pharmacology. 2008; 81:229–235. [PubMed: 18176093]

Sawant Basak A, Byon W, Tseng-Lovering E, Funk C, Wood L, Lin C, Delnomdedieu M, Verhoest P, Parikh V, Cox LM, Miller E, Gao H, Obach RS. Metabolism and clinical pharmacokinetics of 2-methyl-n-(2′-(pyrrolidinyl-1-ylsulfonyl)-n-[1,1′-biphenyl]-4-yl)propran-1-amine : insights into monoamine oxidase- and CYP-mediated disposition by integration of in vitro ADME tools. Xenobiotica. 2013

Schoultz BW, Hjornevik T, Willoch F, Marton J, Noda A, Murakami Y, Miyoshi S, Nishimura S, Arstad E, Drzezga A, Matsunari I, Henriksen G. Evaluation of the kappa-opioid receptor-selective tracer [^{11}C]GR103545 in awake rhesus macaques. European Journal of Nuclear Medicine and Molecular Imaging. 2010; 37:1174–1180. [PubMed: 20157708]

Shirayama Y, Ishida H, Iwata M, Hazama GI, Kawahara R, Duman RS. Stress increases dynorphin immunoreactivity in limbic brain regions and dynorphin antagonism produces antidepressant-like effects. Journal of Neurochemistry. 2004; 90:1258–1268. [PubMed: 15312181]

Talbot PS, Narendran R, Butelman ER, Huang Y, Ngo K, Slifstein M, Martinez D, Laruelle M, Hwang DR. ^{11}C-GR103545, a radiotracer for imaging kappa-opioid receptors in vivo with PET: synthesis and evaluation in baboons. Journal of Nuclear Medicine. 2005; 46:484–494. [PubMed: 15750163]

Tenore PL. Psychotherapeutic benefits of opioid agonist therapy. Journal of Addictive Diseases. 2008; 27:49–65. [PubMed: 18956529]

Tomasi G, Nabulsi N, Zheng MQ, Weinzimmer D, Ropchan J, Blumberg L, Brown-Proctor C, Ding YS, Carson RE, Huang Y. Determination of in vivo Bmax and Kd for ^{11}C-GR103545, an agonist PET tracer for kappa-opioid receptors: a study in nonhuman primates. Journal of Nuclear Medicine. 2013; 54:600–608. [PubMed: 23424192]

Tzourio-Mazoyer N, Landeau B, Papathanassiou D, Crivello F, Etard O, Delcroix N, Mazoyer B, Joliot M. Automated anatomical labeling of activations in SPM using a macroscopic anatomical parcellation of the MNI MRI single-subject brain. Neuroimage. 2002; 15:273–289. [PubMed: 11771995]

Viola P, Wells WM III. Alignment by Maximization of Mutual Information. International Journal of Computer Vision. 1997; 24:137–154.

Highlights

- [^{11}C]GR103545 is a potent and selective kappa opioid receptor (KOR) agonist tracer.
- First human study of [^{11}C]GR103545 was conducted to determine kinetic model.
- Test-retest reliability was good in all regions.
- V_{ND} of [^{11}C]GR103545 was 3 mL/cm^3 from the occupancy plot with naltrexone blocking.
- IC_{50} of the selective KOR antagonist PF-04455242 was estimated as 55 ng/mL.

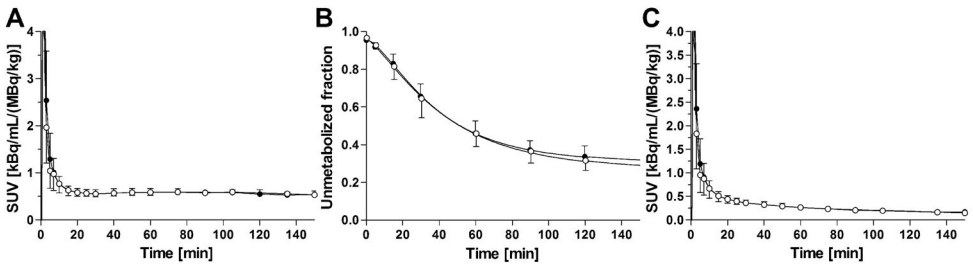

Figure 1.

Mean ± SD of (A) total plasma activity, (B) parent fraction in the plasma, and (C) metabolite-corrected plasma activity over time after injection of [^{11}C]GR103545 in the test (closed circles, n = 11) and retest (open circles, n = 11) scans. Panels (A) and (C) are displayed in SUV unit [concentration / (injected dose/body weight)].

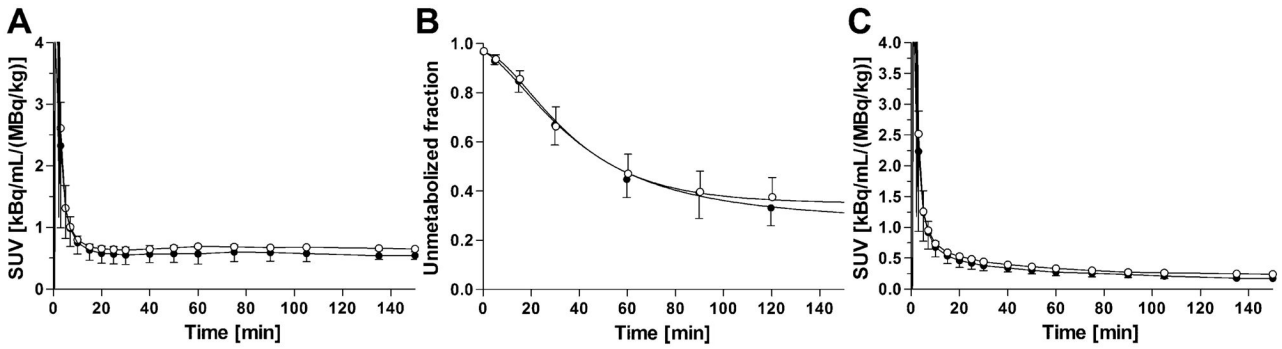

Figure 2.

Mean ± SD of (A) total plasma activity, (B) parent fraction in the plasma, and (C) metabolite-corrected plasma activity over time after injection of [^{11}C]GR103545 in the baseline scan (closed circles, n = 7) and blocking scans with naltrexone (open circles, n = 7). Panels (A) and (C) are displayed in SUV unit [concentration / (injected dose/body weight)].

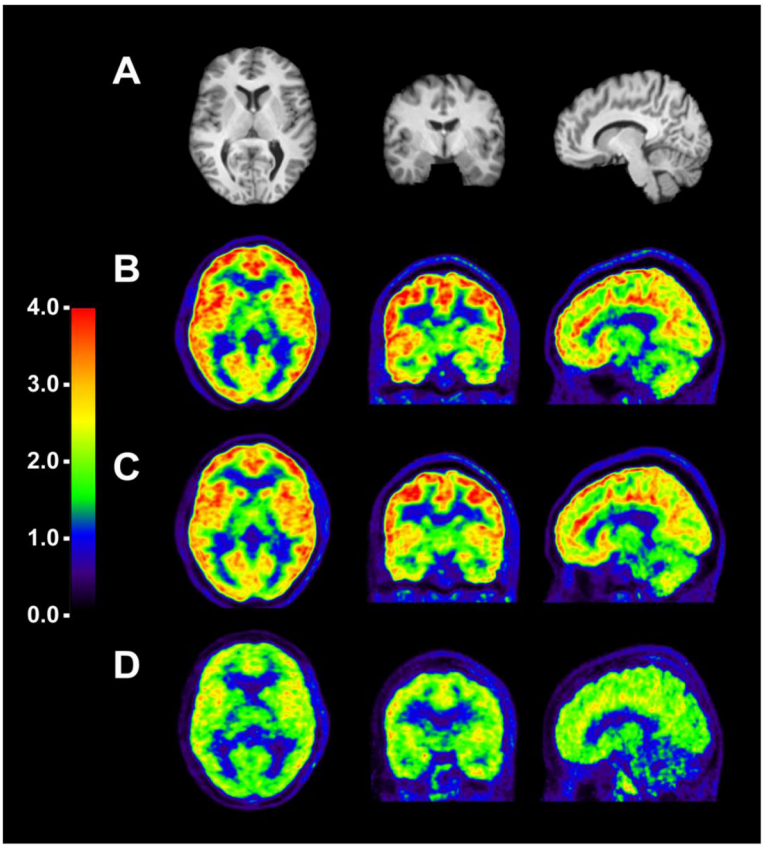

Figure 3.

A: MR images. B-D: typical example of co-registered PET images summed from 30 to 90 min after injection of [^{11}C]GR103545. B: test scan C: retest scan D: post-naltrexone scan. Activity is expressed in SUV [concentration / (injected dose/body weight)].

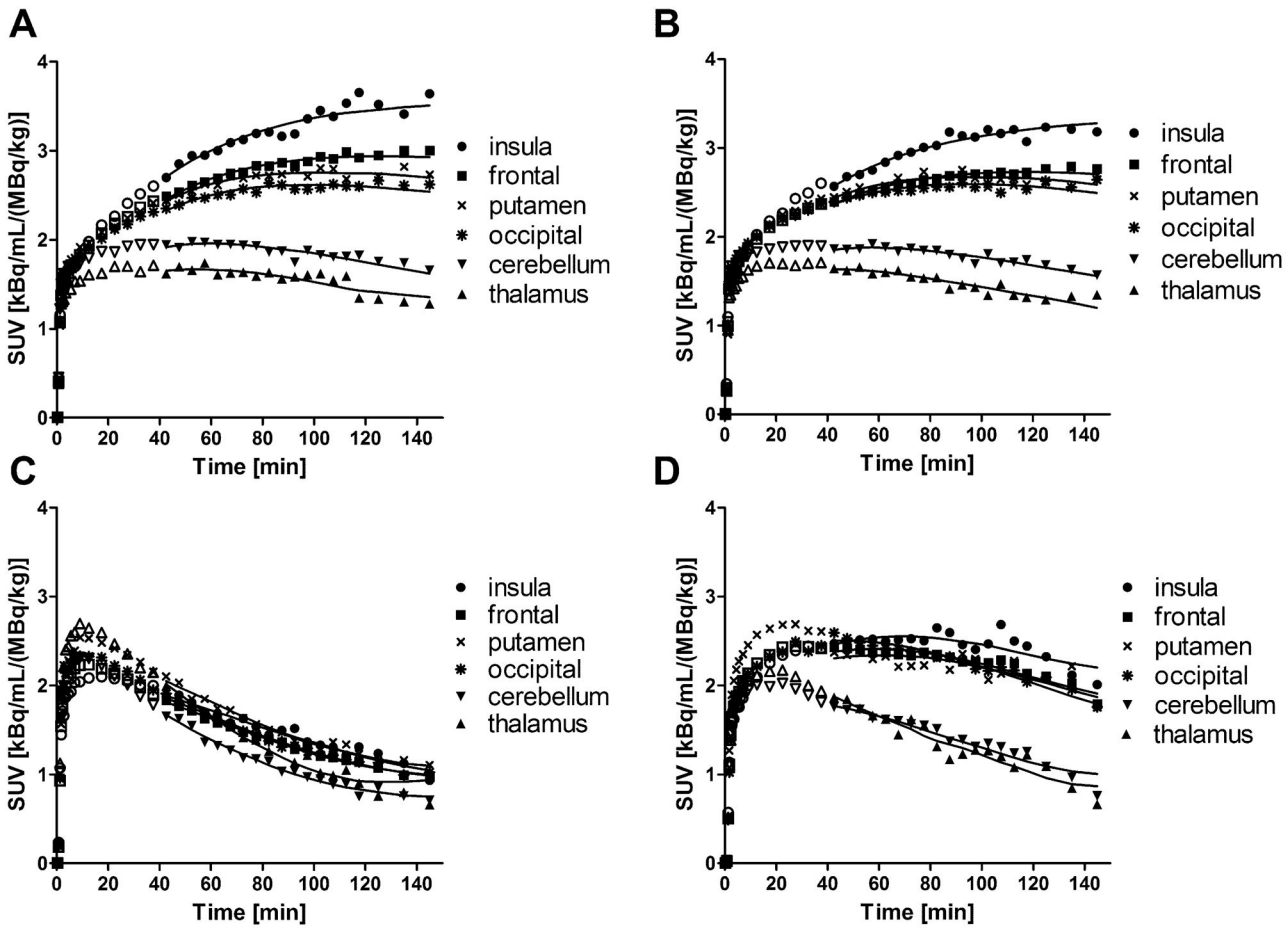

Figure 4.

Typical example of regional time-activity curves in 6 ROIs after injection of [^{11}C]GR103545 at test (A), retest (B), naltrexone blocking (C), and 1.5 h post-PF-04455242 (D) scans. For each region, the symbols correspond to the measured activities and the lines are the values fitted to the MA1 model (t^* = 40 min).

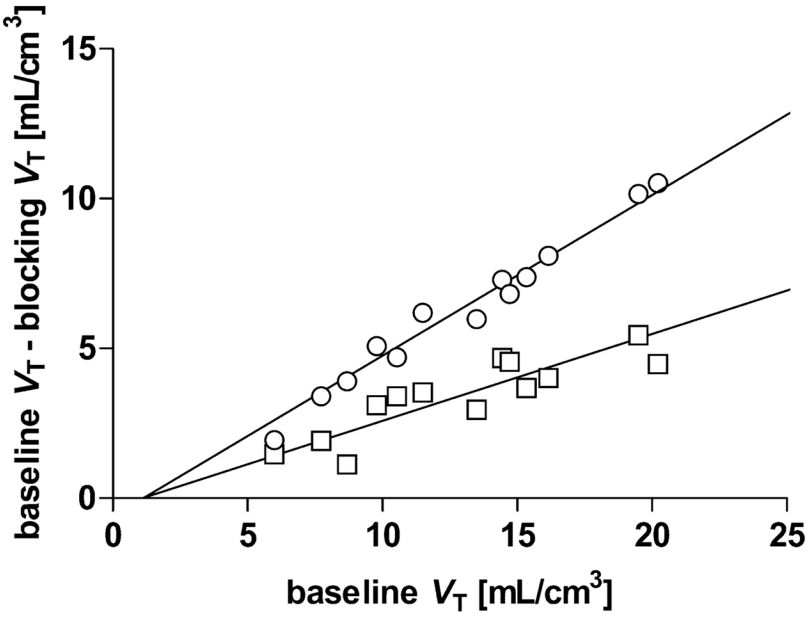

Figure 5.
Example of occupancy plots using distribution volumes from a pair of baseline and blocking scans at 1.5 h (circles) and 8 h (squares) post-PF-04455242.

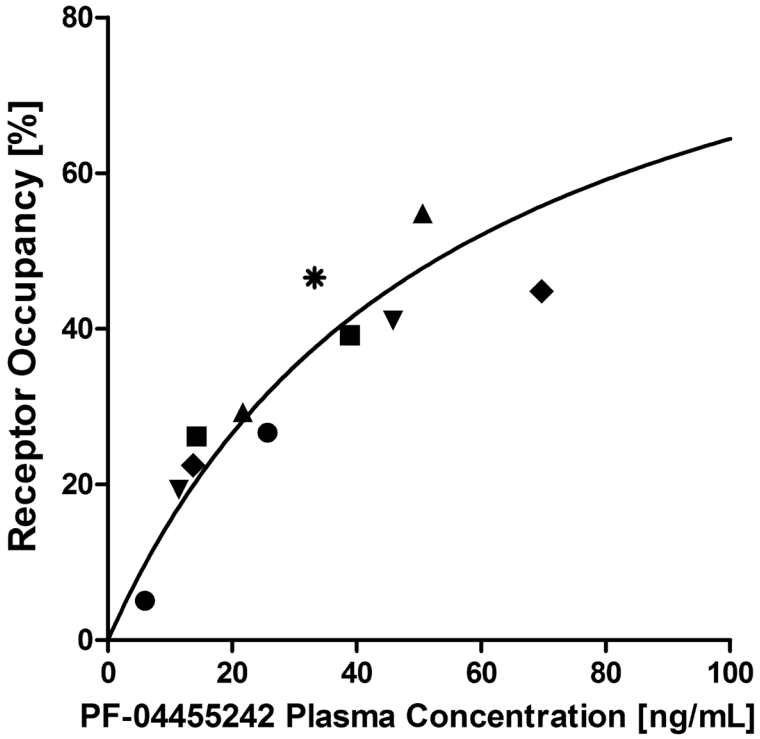

Figure 6.

The relationship between PF-04455242 plasma concentration and KOR occupancy. KOR occupancy values were estimated from the occupancy plot with all regions except for the amygdala. Each symbol corresponds to data from a single subject at post-dose scan #1 (1.5 h after PF-04455242) and post-dose scan #2 (8 h after PF-04455242). The solid curve shows the fit to the single-site occupancy model.

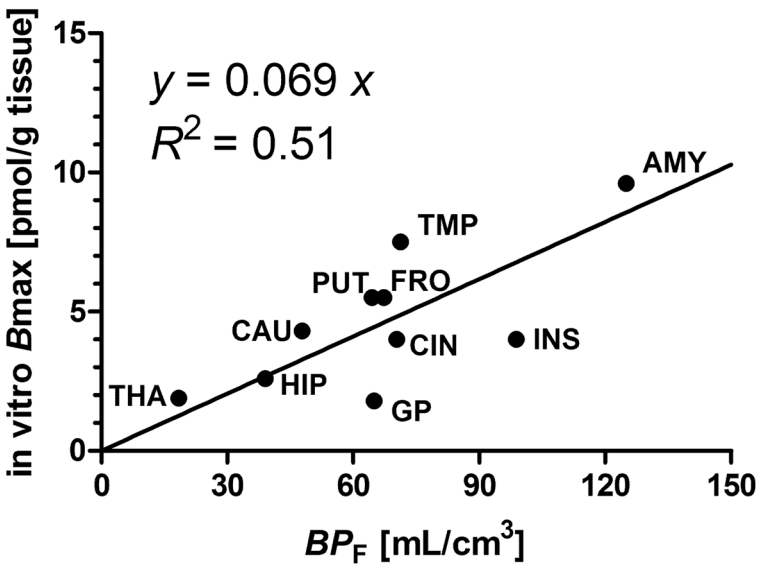

Figure 7.

Correlations between regional BP_F estimates of [^{11}C]GR103545 and *in vitro* KOR B_{max} values from Table 5. Ten ROIs were used: amygdala (AMY), insula (INS), temporal cortex (TMP), frontal cortex (FRO), globus pallidus (GP), putamen (PUT), caudate (CAU), cingulate cortex (CIN), hippocampus (HIP), and thalamus (THA). For CIN, BP_F values were computed as the unweighted average between anterior and posterior values. The regression equation was derived as $B_{max} = 0.069 \times BP_F$ ($R^2 = 0.51$).

Table 1

Subject information and PET scan parameters

Parameter	Test-retest		Blocking with naltrexone		Occupancy with PF-04455242		
	Test (*n* = 11)	Retest (*n* = 11)	Baseline (*n* = 7)	Blocking (*n* = 7)	Baseline (*n* = 6)	1.5 h post-dose (*n* = 6)	8 h post-dose (*n* = 6)
Age (y)	33 ± 8		36 ± 9		37 ± 9		
Body weight (kg)	77.3 ± 11.5		76.9 ± 13.6		80.8 ± 13.6		
Injected dose (MBq)	492 ± 173	516 ± 173	445 ± 243	334 ± 187	392 ± 235	459 ± 184	537 ± 262
Injected mass (μg)	1.17 ± 0.39	1.28 ± 0.32	0.60 ± 0.37	0.44 ± 0.35	1.51 ± 0.40	1.39 ± 0.35	1.20 ± 0.32

Data are mean ± SD.

Table 2

MA1 V_T values for test-retest study

Regions	V_T [mL/cm^3]		V_T/f_P [mL/cm^3]		Minimum scan duration [min]
	Test (%COV)	Retest (%COV)	Test (%COV)	Retest (%COV)	
Amygdala	26.9 (42%)	29.9 (69%)	146 (33%)	164 (78%)	140
Ant. cingulate cortex	25.7 (32%)	23.1 (29%)	142 (26%)	122 (25%)	100
Insula	23.9 (31%)	22.4 (23%)	132 (27%)	119 (21%)	100
Temporal lobe	18.1 (25%)	17.2 (21%)	100 (22%)	92 (20%)	90
Frontal lobe	17.2 (26%)	16.5 (22%)	95 (22%)	88 (19%)	90
Globus pallidus	17.0 (33%)	15.8 (26%)	94 (28%)	84 (26%)	120
Putamen	16.6 (29%)	15.9 (25%)	92 (27%)	85 (24%)	90
Occipital lobe	15.1 (26%)	14.3 (22%)	83 (22%)	76 (19%)	80
Caudate	13.6 (33%)	12.3 (28%)	75 (28%)	65 (24%)	100
Hippocampus	11.5 (30%)	10.9 (23%)	64 (26%)	58 (22%)	110
Cerebellum	10.9 (33%)	10.6 (29%)	61 (32%)	57 (30%)	80
Post. cingulate cortex	10.8 (30%)	10.2 (29%)	60 (26%)	54 (24%)	90
Centrum semiovale	9.4 (32%)	9.4 (32%)	52 (26%)	50 (29%)	120
Thalamus	7.3 (22%)	6.9 (16%)	40 (20%)	37 (15%)	70

COV% is the coefficient of variation (inter-subject variability).

Table 3

Test-retest variability and reproducibility of binding parameters

Regions	V_T			V_T/f_P		
	[a] aTRV [%]	[a] TRV [%]	[b] ICC	[a] aTRV [%]	[a] TRV [%]	[b] ICC
Amygdala	41	−3 ± 54	0.05	41	0 ± 52	0.11
Ant. cingulate cortex	19	10 ± 25	0.71	21	14 ± 25	0.51
Insula	16	5 ± 21	0.67	18	9 ± 21	0.53
Temporal lobe	12	4 ± 14	0.82	14	8 ± 16	0.67
Frontal lobe	11	3 ± 15	0.82	14	7 ± 15	0.71
Globus pallidus	15	6 ± 18	0.79	16	10 ± 18	0.74
Putamen	11	3 ± 16	0.84	14	7 ± 17	0.73
Occipital lobe	12	4 ± 15	0.81	15	8 ± 16	0.65
Caudate	15	8 ± 17	0.82	19	13 ± 18	0.68
Hippocampus	17	4 ± 21	0.68	16	8 ± 20	0.58
Cerebellum	8	2 ± 12	0.92	13	6 ± 14	0.90
Post. cingulate cortex	13	5 ± 14	0.90	17	9 ± 18	0.72
Centrum semiovale	12	1 ± 15	0.92	13	5 ± 16	0.86
Thalamus	9	4 ± 12	0.77	12	8 ± 12	0.69

[a] TRV = $(p_{test}-p_{retest})/(p_{test}+p_{retest})\times 2$, and aTRV is the absolute value of TRV

[b] ICC = (BSMSS-WSMSS) / (BSMSS+WSMSS) where BSMSS is the mean sum of squares between subjects and WSMSS is the mean sum of squares within subjects

Table 4

MA1 V_T for baseline-blocking experiments

Regions	V_T [mL/cm^3]			
	[a] Baseline (%COV)	[b] Blocking with naltrexone (%COV)	[c] Occupancy with PF-04455242 (%COV)	
			1.5 h post-dose	8 h post dose
Amygdala	28.17 (50%)	7.05 (39%)	12.48 (35%)	18.94 (22%)
Ant. cingulate cortex	22.66 (23%)	6.14 (32%)	13.56 (26%)	17.06 (22%)
Insula	22.75 (20%)	6.31 (34%)	12.39 (27%)	16.19 (18%)
Temporal lobe	17.24 (18%)	5.52 (29%)	9.58 (21%)	12.17 (15%)
Frontal lobe	16.45 (18%)	5.19 (29%)	9.83 (23%)	12.17 (16%)
Globus pallidus	18.34 (54%)	5.28 (30%)	9.19 (29%)	11.27 (30%)
Putamen	15.85 (22%)	5.38 (31%)	8.88 (24%)	10.73 (20%)
Occipital lobe	14.51 (16%)	5.11 (27%)	8.39 (18%)	10.29 (15%)
Caudate	11.70 (33%)	4.05 (25%)	6.23 (32%)	7.47 (24%)
Hippocampus	10.38 (21%)	4.72 (27%)	6.83 (27%)	7.31 (19%)
Cerebellum	9.63 (27%)	3.76 (25%)	6.24 (28%)	7.01 (19%)
Post cingulate cortex	10.67 (19%)	4.41 (27%)	6.34 (28%)	7.40 (26%)
Centrum semiovale	9.34 (16%)	4.36 (29%)	5.57 (21%)	6.20 (27%)
Thalamus	7.00 (19%)	4.27 (28%)	4.80 (24%)	4.90 (24%)

[a] Baseline scans (n = 13)

[b] Blocking scan with naltrexone (n = 7)

[c] Occupancy scans at 1.5 h (n = 5) and 8 h (n = 4) after oral administration of PF-04455242 (30 mg)

Table 5

Regional in vitro B_{max} values

Regions	B_{max} [fmol/mg tissue]
Amygdala	9.6
Cingulate cortex	4.0
Insula	4.0
Temporal lobe	7.5
Frontal lobe	5.5
Globus pallidus	1.8
Putamen	5.5
Caudate	4.3
Hippocampus	2.6
Thalamus	1.9